The Astrophysical Journal Letters, 873:L7 (9pp), 2019 March 1 https://doi.org/10.3847/2041-8213/ab0651

The K Dwarf Advantage for Biosignatures on Directly Imaged Exoplanets

Giada N. Arney[1,2,3]
[1] Planetary Systems Laboratory, NASA Goddard Space Flight Center, Greenbelt, MD 20771, USA; giada.n.arney@nasa.gov
[2] NASA NExSS Virtual Planetary Laboratory, P.O. Box 351580, Seattle, WA 98195, USA
[3] Sellers Exoplanet Environments Collaboration, NASA Goddard Space Flight Center, Greenbelt, MD 20771, USA
Received 2018 December 21; revised 2019 February 11; accepted 2019 February 12; published 2019 March 6

Abstract

Oxygen and methane are considered to be the canonical biosignatures of modern Earth, and the simultaneous detection of these gases in a planetary atmosphere is an especially strong biosignature. However, these gases may be challenging to detect together in the planetary atmospheres because photochemical oxygen radicals destroy methane. Previous work has shown that the photochemical lifetime of methane in oxygenated atmospheres is longer around M dwarfs, but M dwarf planet habitability may be hindered by extreme stellar activity and evolution. Here, we use a 1D photochemical-climate model to show that K dwarf stars also offer a longer photochemical lifetime of methane in the presence of oxygen compared to G dwarfs. For example, we show that a planet orbiting a K6V star can support about an order of magnitude more methane in its atmosphere compared to an equivalent planet orbiting a G2V star. In the reflected-light spectra of worlds orbiting K dwarf stars, strong oxygen and methane features could be observed at visible and near-infrared wavelengths. Because K dwarfs are dimmer than G dwarfs, they offer a better planet-star contrast ratio, enhancing the signal-to-noise ratio (S/N) possible in a given observation. For instance, a 50 hr observation of a planet at 7 pc with a 15 m telescope yields S/N = 9.2 near 1 μm for a planet orbiting a solar-type G2V star, and S/N = 20 for the same planet orbiting a K6V star. In particular, nearby mid-late K dwarfs such as 61 Cyg A/B, Epsilon Indi, Groombridge 1618, and HD 156026 may be excellent targets for future biosignature searches.

Key words: planets and satellites: atmospheres – planets and satellites: composition – planets and satellites: terrestrial planets

1. Introduction

One of the most profound scientific questions that could be answered in the near future is whether there is life on other planets. Future telescopes will seek remotely detectable signs of life, or biosignatures, in exoplanet atmospheres. The most studied approach to biosignature search strategies is detection of an atmosphere in chemical disequilibrium (e.g., Lovelock 1965; Hitchcock & Lovelock 1967; Sagan et al. 1993; Kaltenegger et al. 2007; Krissansen-Totton et al. 2016, 2018; Schwieterman et al. 2018b). For modern Earth, the largest overall disequilibrium is caused by the simultaneous presence of oxygen (O_2), atmospheric nitrogen (N_2), and liquid water (H_2O), which would react to form nitrate and hydrogen ions in equilibrium (Krissansen-Totton et al. 2016). Unfortunately, N_2 may be challenging to observe in direct spectral observations (Schwieterman et al. 2015), so other directly delectable biosignatures should be sought.

The "canonical" biosignature disequilibrium pairing for modern Earth is the simultaneous presence of O_2 and methane (CH_4), whose atmospheric abundances are orders of magnitude away from equilibrium values (Lovelock 1965; Hitchcock & Lovelock 1967). These gases, which both produce spectral features at visible and near-infrared (NIR) wavelengths, will be high-priority gases sought in future biosignature searches. However, despite their importance as biosignatures, oxygen and methane have not always been detectable in Earth's atmosphere over our planet's geological history. Briefly, we will review the history of oxygen and methane in Earth's atmosphere in order to provide context and motivation for the search for these gases on exoplanets.

Oxygenic photosynthesis, the dominant metabolism on our planet today, probably evolved on Earth about 3 billion years (or giga-annum (Ga)) ago (Planavsky et al. 2014a), and potentially as early as 3.7 Ga (Rosing & Frei 2004). Because it uses cosmically ubiquitous compounds (H_2O, CO_2, starlight) and has a high energy yield, this metabolism may be incentivized to evolve elsewhere.

However, atmospheric oxygenation depends not only on O_2 production, but also on the competition between O_2 sources and sinks. While oxygenic photosynthesis likely existed earlier, it was not until roughly 2.3 Ga (the start of the Proterozoic geological eon) that atmospheric oxygen levels rose during the "Great Oxygenation Event." However, oxygen levels were likely variable throughout the Proterozoic, and in the mid-Proterozoic (2.0–0.7 Ga), atmospheric oxygen abundance may have been much lower than modern levels, possibly lower than 0.1% of the present atmospheric level (PAL; Planavsky et al. 2014b). At an O_2 level this low, oxygen itself cannot be observed directly in the planet's spectrum, but it might be indirectly inferred by detecting its photochemical byproduct, ozone (O_3), which produces a strong spectral feature at ultraviolet (UV) wavelengths even when O_2 itself is spectrally invisible.

Methane also has a long history of biogenic production on Earth. Methanogenesis, a simple anaerobic metabolism that produces methane from CO_2 and H_2, is rooted deeply in Earth's tree of life (Woese & Fox 1977; Ueno et al. 2006). Methanogenesis may even have evolved as early as during the Hadean geological period (prior to 3.8 Ga, a time when

Earth's geological record has nearly entirely vanished; Battistuzzi et al. 2004). While CH_4 also has geological sources, most of the CH_4 in Earth's atmosphere today is biogenic (Etiope & Sherwood Loller 2013), and this was likely also the case for early Earth (Kharecha et al. 2005).

Despite the continual production of biogenic O_2 and CH_4 on Earth for billions of years, these gases may not have produced simultaneously detectable spectral features over our planet's history (Olson et al. 2016; Reinhard et al. 2017). Methane is readily destroyed by oxygen radicals in an atmosphere containing oxygen around a G2V star. The dominant sink of CH_4 on Earth starts with photodissociation of O_3 (which itself forms from O_2 photochemistry):

$$O_3 + h\nu \longrightarrow O_2 + O^1D \quad \text{(R1)}$$

$$O^1D + H_2O \longrightarrow 2OH \quad \text{(R2)}$$

$$CH_4 + OH \longrightarrow CH_3 + H_2O. \quad \text{(R3)}$$

Because this mechanism is driven by photochemistry, different host stars may lead to different photochemical outcomes. Segura et al. (2005) showed that CH_4 has a longer photochemical lifetime in the atmospheres of Earth-like planets orbiting M dwarf stars, which produce less radiation compared to the Sun at 200–350 nm, where O_3 is photolyzed. This increases the CH_4 photochemical lifetime from 10 yr for a planet orbiting the Sun to about 200 yr. It may therefore be easier to simultaneously detect CH_4 and O_2 for planets around M dwarfs (see also, e.g., Meadows et al. 2018).

Potentially habitable planets orbiting M dwarfs will likely be targeted by the *James Webb Space Telescope* and future large ground-based observatories. Unfortunately, the habitability of M dwarf planets may be hindered by a number of complications including: extreme water loss during the extended superluminous pre-main sequence phase (Luger & Barnes 2015), high X-ray luminosities (Shkolnik & Barman 2014), and frequent energetic flares that may cause severe atmospheric loss (Owen & Mohanty 2016; Airapetian et al. 2017; Garcia-Sage et al. 2017).

Recently, the *Exoplanet Science Strategy* Report (National Academies of Sciences & Medicine 2018) recommended that NASA "lead a large strategic direct imaging mission capable of measuring the reflected-light spectra of temperature terrestrial planets orbiting Sun-like stars." Planets orbiting F, G, and K dwarfs (i.e., "Sun-like stars") do not face the multiple challenges to habitability posed by M dwarfs, and they may therefore represent our best chance of discovering other planets similar to Earth. NASA has directed studies of two observatories for consideration in the astrophysics 2020 decadal survey that would be capable of directly observing temperate, Earth-sized exoplanets around Sun-like stars: the Large UV Optical Infrared surveyor (LUVOIR[4]) and the Habitable Exoplanet Observatory (HabEx[5]).

Compared to F and G dwarfs, K dwarfs offer certain advantages as habitable planet hosts: they are more abundant than G and F dwarfs, comprising about 12% of the main sequence stellar population (G dwarfs comprise about 8%, while F dwarfs comprise a paltry 3%); their lifetimes are longer than F and G dwarfs (17–70 billion years for K dwarfs, compared to 10 billion years for the Sun); and the planet-star contrast ratio is better for K dwarfs than for F and G dwarfs (a K2V star is only about one-third as luminous as a G2V star, and a K6V star is only about one-tenth as luminous), making their planets easier to observe via direct imaging. Many advantages of K dwarfs as habitable planet hosts are discussed in detail in Cuntz & Guinan (2016).

Additionally, compared to M dwarfs, K dwarfs are less active, and their pre-main sequence phases are shorter (<0.1 Gyr compared to up to 1 Gyr for M dwarfs; Luger & Barnes 2015). Recently, Richey-Yowell et al. (2019) measured the near-UV (NUV), far-UV (FUV), and X-ray evolution of K dwarf stars in moving groups aged from 10 to 625 Myr, finding that young planets orbiting K dwarfs are subjected to 5–50 times lower UV and X-ray fluxes compared to planets orbiting early M dwarfs, and 50–1000 times lower fluxes compared to planets orbiting late M dwarfs. Richey-Yowell et al. (2019) also found that K dwarf FUV and X-ray fluxes decrease after ~100 Myr, compared to ~650 Myr for M dwarfs, which may have implications for early habitability and atmospheric evolution for planets around these different types of stars. The UV environment of a given host star is critical to consider when studying planetary habitability and photochemistry.

Here, we explore an additional advantage for K dwarfs: the hypothesis that like M dwarfs, K dwarf stellar UV spectra will result in longer photochemical lifetimes for methane in oxygenated atmospheres. Previous photochemical modeling efforts of Earth-like planets orbiting K dwarfs have explored this effect (Segura et al. 2003; Rugheimer et al. 2013; Rugheimer & Kaltenegger 2018), but there are differences between these studies and ours. This new analysis using a recently upgraded photochemical model focuses explicitly on determining which parts of the CH_4/O_2/stellar spectrum parameter space produce simultaneously observable CH_4 and O_2 spectral features for the Sun and several K dwarfs. We allow Earth history to bound parts of the explored parameter space. However, we also simulate atmospheres that are not representative of any period of Earth history to consider exoplanets with different evolutionary paths. In addition, we discuss the implications of these results in the context of possible future exoplanet observatories, and we consider which of the nearby K dwarf stars may be the best targets for future biosignature searches. By understanding the "K dwarf advantage," we improve our chances of selecting the best targets for biosignature searches with future observatories.

2. Methods

To simulate our atmospheres, we use a coupled 1D photochemical-climate model called Atmos, which is described in Arney et al. (2016). Its photochemical module is based on a photochemical code originally developed by Kasting et al. (1979) and significantly updated and modernized as described in Zahnle et al. (2006). The photochemical module has recently been updated as described in Lincowski et al. (2018) with an expanded and higher-resolution wavelength grid; and updated cross sections, quantum yields, and reaction rates. Tests comparing the upgraded model used here to the previous version suggest that the previous version may overestimate CH_4 abundances for the types of atmospheres that we simulate here by up to 50%. This upgraded model has been validated on Earth and Venus as described in Lincowski et al. (2018). The climate module of Atmos was originally developed by Kasting & Ackerman (1986), and like the photochemical model has evolved considerably since this first incarnation. This climate

[4] https://asd.gsfc.nasa.gov/luvoir/
[5] https://www.jpl.nasa.gov/habex/

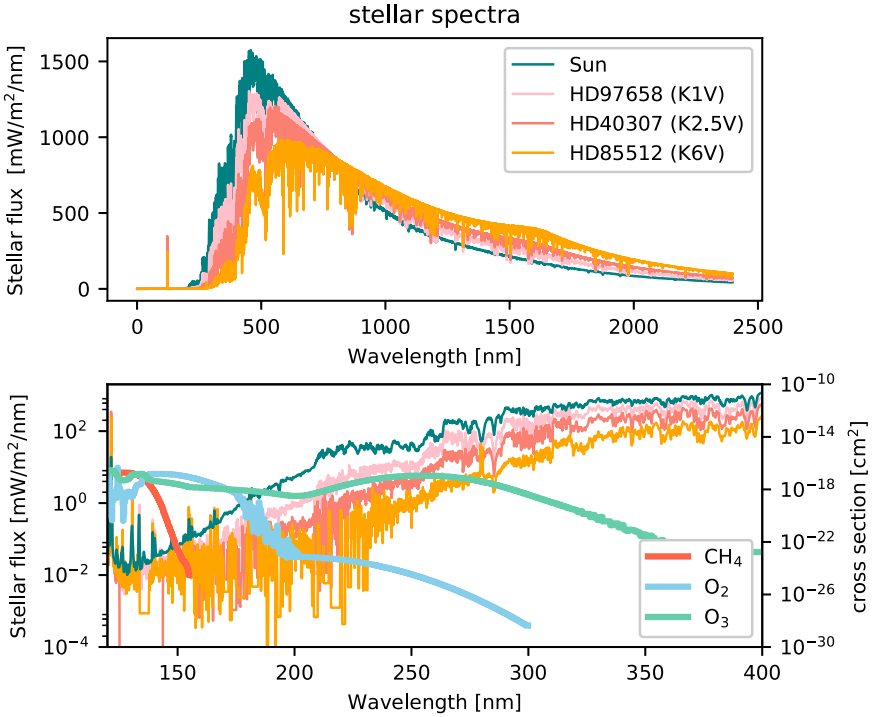

Figure 1. Top panel: stellar spectra used in our simulations. Bottom panel: the stellar UV wavelengths. Also shown in the bottom panel are UV cross sections of CH_4, O_2, and O_3 (right *y*-axis).

module has recently been used to study, e.g., habitable zone (HZ) boundaries (Kopparapu et al. 2013).

We simulate planets orbiting the K dwarf stars in the Measurements of the Ultraviolet Spectral Characteristics of Low-mass Exoplanetary Systems (MUSCLES) treasury survey (France et al. 2016; Loyd et al. 2016; Youngblood et al. 2016): HD 97658 (K1V), HD 40307 (K2.5V), and HD 85512 (K6V). We also include the Sun (Chance & Kurucz 2010) for comparison. These spectra and stellar properties are provided in Figure 1 and the top rows of Table 1.

A planet receiving the same total insolation (i.e., incident solar energy, S_o) that modern Earth receives from the Sun would place it inside the inner edge of the conservative HZ for a K6V star (Kopparapu et al. 2013). Therefore, to be conservative, we set the orbital distances of each planet around each of their stars to be where they receive 0.7 times the modern Earth-equivalent insolation ($0.7 \times S_o$, see Table 1). This allows each planet to sit well within its star's HZ, allowing our climate simulations to avoid extreme warming in the methane-rich atmospheres that we simulate.

For our simulated atmospheres, we vary the oxygen partial pressure (pO_2) between 10^{-3} and 0.21 bar (equivalent to O_2 mixing ratios of 10^{-3} and 0.21), which brackets higher Proterozoic-like O_2 levels and the modern O_2 abundance. We exclude the lower mid-Proterozoic oxygen estimates ($pO_2 \leqslant 10^{-4}$ bar, Planavsky et al. 2014a) because our goal is to explore the phase space of atmospheres with directly detectable oxygen and methane, but the lowest oxygen estimates for the Proterozoic do not produce directly detectable O_2 spectral features. We vary CH_4 fluxes (fCH_4) at the surface of the model between 7×10^{10} and 10^{12} molecules cm^{-2} s^{-1}. This brackets the modern methane flux to roughly an order of magnitude greater methane than is produced on modern Earth. Note that higher CH_4 fluxes than the modern flux may be possible for Archean Earth (Kharecha et al. 2005), and this range of fluxes is sufficiently high enough that abiotic production at these rates is implausible on an exoplanet (Krissansen-Totton et al. 2018). We do not explore methane flux levels less than the modern production rate because lower fluxes do not generate strongly detectable methane spectral features for the oxygenated atmospheres that we simulate. Our upper bound for CH_4 production allows us to consider an optimistic case for an exoplanet with much more vigorous biotic methane production than Earth.

The partial pressure of CO_2 (pCO_2) is set at 0.01 bar to provide greenhouse warming in our coupled climate-photochemical model for insolation of $0.7 \times S_o$. A total surface pressure of 1 bar is assumed for all atmospheres.

Spectra are generated using the Spectral Mapping Atmospheric Radiative Transfer Model (Meadows & Crisp 1996), a 1D line-by-line fully multiple scattering radiative transfer model. The surface albedo in our spectral model uses a composite average of 65.6% seawater, 23.1% soil/desert, and 11.3% snow/ice as described in Meadows et al. (2018). Patchy clouds in our disk-integrated spectra are included by constructing weighted averages with 50% clear sky, 25% cirrus clouds, and 25% stratocumulus clouds. Coronagraph simulations of observations with possible future telescopes are generated with the model described in Robinson et al. (2016) with updates described in Meadows et al. (2018). An online version of this model is available at the LUVOIR website.[6]

3. Results

Figure 2 shows how later host star types lead to increasing concentrations of methane as a function of methane flux and oxygen concentration. For our analysis, we select three points from this parameter space for each star as interesting case studies for deeper analysis. Where possible, we consider atmospheres that are consistent with the biogeochemical

[6] https://asd.gsfc.nasa.gov/luvoir/tools/

Table 1
Key Stellar Properties and Resulting Planetary Atmospheric Properties

	Sun (G2V)	HD 97658 (K1V)	HD 40307 (K2.5V)	HD 85512 (K6V)
Temperature (K)	5778	4991	4977	4759
Mass (M_{Sun})	1	0.75	0.75	0.69
Luminosity (L_{Sun})	1	0.3	0.23	0.13
Planet-star separation (au)	1.2	0.65	0.57	0.42
CH_4 surface mixing ratio	2.4×10^{-5}	3.7×10^{-5}	7.0×10^{-5}	2.2×10^{-4}
Case 1, 2, 3	9.0×10^{-6}	1.3×10^{-5}	2.2×10^{-5}	5.0×10^{-5}
	8.7×10^{-5}	1.3×10^{-4}	2.5×10^{-4}	8.1×10^{-4}
CH_4 photolysis rate (s^{-1})	3.7×10^{9}	1.4×10^{10}	2.8×10^{10}	7.0×10^{10}
Case 1, 2, 3	3.0×10^{8}	1.4×10^{9}	3.1×10^{9}	6.6×10^{9}
	9.1×10^{8}	8.3×10^{9}	2.3×10^{10}	6.8×10^{10}
CH_4 column density	4.9×10^{20}	7.6×10^{20}	1.4×10^{21}	4.7×10^{21}
Case 1, 2, 3	1.8×10^{20}	2.7×10^{20}	4.6×10^{20}	9.4×10^{20}
	1.8×10^{21}	2.6×10^{21}	5.0×10^{21}	1.7×10^{22}
O_2 photolysis rate (s^{-1})	1.3×10^{12}	4.7×10^{11}	3.1×10^{11}	1.8×10^{11}
Case 1, 2, 3	2.3×10^{12}	9.2×10^{11}	6.9×10^{11}	4.8×10^{11}
	3.6×10^{12}	1.2×10^{12}	8.0×10^{11}	4.8×10^{11}
O_2 surface flux (molec s^{-1} cm^{-2})	7.7×10^{11}	7.8×10^{11}	7.9×10^{11}	7.8×10^{11}
Case 1, 2, 3	5.4×10^{11}	5.4×10^{11}	5.4×10^{11}	5.5×10^{11}
	2.8×10^{12}	2.8×10^{12}	2.9×10^{12}	2.9×10^{12}
O_3 photolysis rate (s^{-1})	1.3×10^{15}	4.3×10^{14}	1.3×10^{14}	2.2×10^{13}
Case 1, 2, 3	1.9×10^{15}	1.0×10^{15}	4.9×10^{14}	1.7×10^{14}
	1.5×10^{15}	6.9×10^{14}	2.7×10^{14}	5.9×10^{13}
O_3 column density	3.3×10^{18}	1.5×10^{18}	5.1×10^{17}	1.3×10^{17}
Case 1, 2, 3	7.2×10^{18}	4.7×10^{18}	2.7×10^{18}	1.3×10^{18}
	5.2×10^{18}	2.9×10^{18}	1.3×10^{18}	4.0×10^{17}

Note. Note that the planet for the Earth–Sun system is assumed to be at 1.2 au because we assume that all planets receive 0.7× Earth's insolation to place all of the K dwarf planets in the habitable zone.

calculations of Olson et al. (2016), which describes how methane fluxes to the atmosphere are impacted by pO_2.

1. "Case 1" represents a Proterozoic-like planet consistent with Olson et al. (2016) with $pO_2 = 5 \times 10^{-3}$ bar and $fCH_4 = 3 \times 10^{11}$ molecules cm^{-2} s^{-1}.
2. "Case 2" is a quasi-modern Earth-like planet that is also consistent with the calculations of Olson et al. (2016) with $pO_2 = 0.1$ bar and $fCH_4 = 1 \times 10^{11}$ molecules cm^{-2} s^{-1}.
3. "Case 3" represents a type of exoplanet with modern Earth O_2 and significantly higher CH_4 production than Earth: $pO_2 = 0.21$ bar, $fCH_4 = 1 \times 10^{12}$ molecules cm^{-2} s^{-1}. This planet allows us to examine an optimistic case of high biological production of both of these gases on a world that is different from Earth.

The K dwarfs studied here produce less radiation than the Sun at almost all UV wavelengths, so O_3 is less readily photolyzed (Figure 1, bottom panel), generating fewer oxygen radicals and allowing enhanced accumulation of CH_4. Interestingly, the K dwarf planets also generate less O_3 to begin with compared to the planets orbiting the Sun because they also less readily photolyze O_2, which is needed to generate O_3 (Table 1). As shown in Table 1, photolysis of O_2 is almost an order of magnitude slower for planets orbiting the K6V star compared to equivalent planets orbiting the Sun. As a result of these factors, the K dwarf planets have more methane than the planets orbiting the Sun, with methane levels increasing toward later type K dwarf stars. A planet orbiting the K6V star used here can have about an order of magnitude more CH_4 in an oxygenated atmosphere compared to an equivalent planet around the Sun (Table 1). Additionally, our results show a trend of increasing CH_4 toward higher oxygen mixing ratios, peaking for most stars at about $pO_2 = 10^{-1.3}$ bar, which is attributable to shielding of CH_4 from photolysis by O_2 and O_3 (e.g., Olson et al. 2016, and note the overlap in the UV cross sections of CH_4 with O_2 and O_3 in Figure 1).

While planets orbiting K dwarfs have more CH_4 relative to equivalent planets around G dwarfs, M dwarfs offer the potential for even more CH_4 in equivalent atmospheres because they produce even lower levels of radiation at the UV wavelengths needed for ozone photolysis (Segura et al. 2005; Meadows et al. 2018). For instance, Segura et al. (2005) found that methane levels increased by over two orders of magnitude for modern Earth-like planets orbiting the M dwarfs AD Leo and GJ 436C compared to planets orbiting the Sun. However, M dwarfs may be problematic habitable planet hosts for the reasons discussed in Section 1.

Table 1 also shows the O_2 surface flux required to produce the constant O_2 mixing ratios selected from our parameter space to represent Cases 1, 2, and 3. In each of these cases, the O_2 flux is controlled by the O_2 mixing ratio selected and the amount of reductants in the atmosphere. In each of these cases, the O_2 fluxes are larger than the CH_4 surface fluxes. Biogenic methane fluxes larger than the oxygen fluxes may be difficult to sustain on planets with primary productivities driven by oxygenic photosynthesis (Zerkle et al. 2012), so these atmospheres are consistent with this constraint.

Future direct imaging observatories being studied, such as LUVOIR and HabEx, are baselined to be able to observe exoplanets to a longest wavelength of 2 μm (at longer

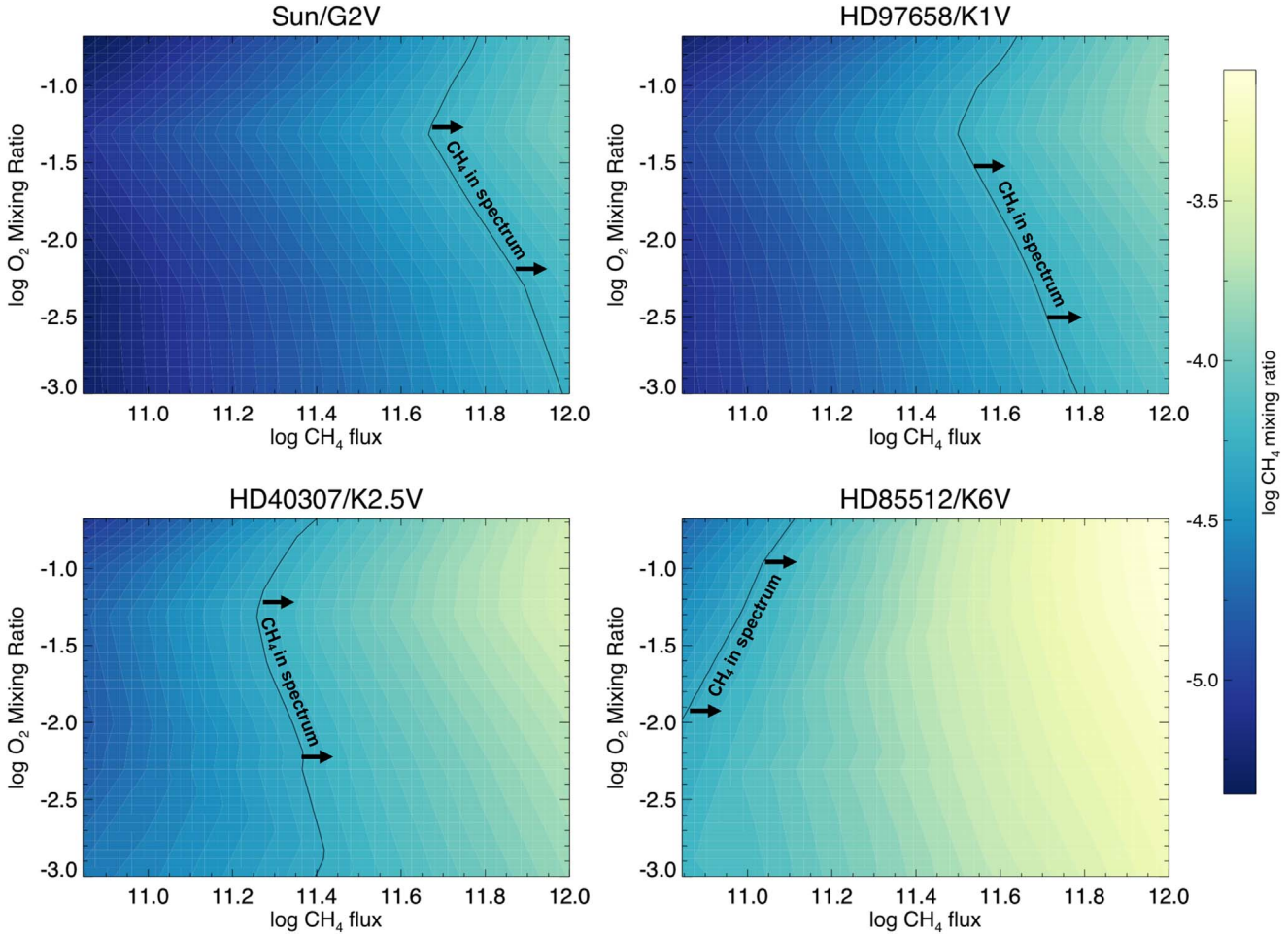

Figure 2. Planetary surface methane mixing ratios as a function of stellar type, methane flux at the planet surface, and surface O_2 mixing ratio. Lower-mass stars with less UV flux generate fewer photochemical oxygen radicals, which leads to more methane present in their planets' atmospheres. The solid line indicates atmospheres with methane mixing ratios of 5×10^{-5}, which allows for methane features to begin to become apparent in the spectrum near 1.4 and 1.15 μm. We consider atmospheres to the right of this line especially useful candidates for methane detection in direct imaging.

wavelengths, thermal radiation from the telescope swamps the planet signal). Methane begins to become weakly apparent in the planet spectrum at 1.7 μm for mixing ratios of about 1×10^{-6} bar (this is roughly the concentration of CH_4 in modern Earth's atmosphere), but detecting CH_4 at this low abundance would be extremely challenging (e.g., Reinhard et al. 2017). Even at higher methane abundances, observing 1.7 μm may be difficult because longer wavelengths are vulnerable to falling inside the telescope's inner working angle (IWA) (see Section 4), especially for K dwarf planets that orbit closer to their stars than planets in the HZs of G dwarfs.

At a methane mixing ratio of roughly 5×10^{-5} bar, CH_4 features near 1.4 and 1.15 μm begin to become weakly apparent in the spectrum. Therefore, we consider CH_4 mixing ratios $>5 \times 10^{-5}$ bar to be best for detecting methane with direct imaging observatories that can observe wavelengths <2 μm as these wavelengths are less likely to be cut off by the IWA. We indicate this part of parameter space with the solid line on each panel in Figure 2: atmospheres to the right of this line have CH_4 mixing ratios $>5 \times 10^{-5}$ bar.

Several of the atmospheres that we simulate have high enough oxygen and methane concentrations that both of these gases produce prominent spectral features at visible and NIR wavelengths accessible to direct imaging observatories. Figure 3 shows spectra for Cases 1, 2, and 3 for planets orbiting the Sun, which has the weakest CH_4 features, and for planets orbiting the K6V star, which has the strongest CH_4 features. Notably, Cases 1 and 3 allow access to methane features near and shortward of 1 μm for the K6V planets. Interestingly, because O_3 production is diminished by about an order of magnitude for the K6V planets compared to the planets orbiting the Sun, the O_3 Chappuis band centered near 0.6 μm is not apparent for the K6V planets. The UV O_3 Hartley–Huggins band is still visible in all spectra for $\lambda < 0.3$ μm, and this band is notably not saturated for the Case 1 K6V planet. For planets with even lower O_2 amounts than we simulate here, such as atmospheres with $\leqslant$0.1% PAL O_2 possibly representative of the mid-Proterozoic (Planavsky et al. 2014b), O_2 itself will be extremely difficult to observe. Therefore, access to UV wavelengths will be particularly important for observing O_3 and establishing the presence of oxygen in such planets' atmospheres (Schwieterman et al. 2018a).

4. Discussion

The exoplanet revolution has already surprised us with the discovery of worlds not represented in our solar system (e.g., hot Jupiters and super Earths) and the knowledge that there are entire systems of small planets on our cosmic doorstep (e.g., the TRAPPIST-1 seven-planet system, orbiting an M8V star at

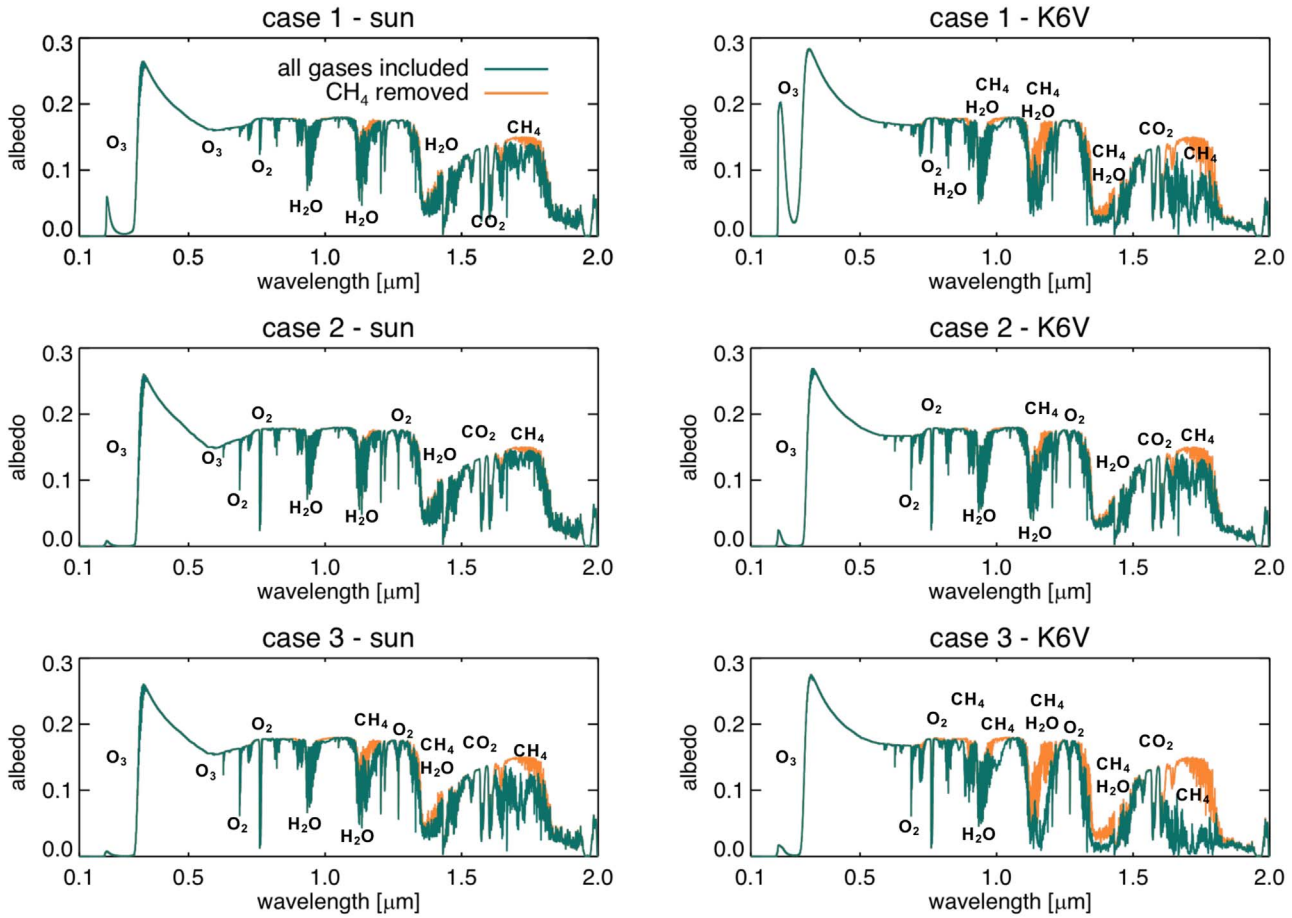

Figure 3. Spectra of selected parts of parameter space for the solar-type and the K6V planets. In all cases, methane features are stronger for the planets around the K6V star. The teal colored spectra include all gases; methane has been removed from the orange spectra to so that its absorption features can be easily seen. Case 1 is the Proterozoic-like planet ($pO_2 = 5 \times 10^{-3}$ bar and $fCH_4 = 3 \times 10^{11}$ molecules cm^{-2} s^{-1}), Case 2 is the quasi-modern planet ($pO_2 = 0.1$ bar and $fCH_4 = 1 \times 10^{11}$ molecules cm^{-2} s^{-1}), and Case 3 is the highest CH_4/highest O_2 scenario ($pO_2 = 0.21$ bar, $fCH_4 = 1 \times 10^{12}$ molecules cm^{-2} s^{-1}).

12 pc; Gillon et al. 2017). By observational necessity, most of the current and near-future observations of exoplanets focus on M dwarfs, but these planets' prospects for habitability may be imperiled by high stellar activity levels and a lengthy superluminous pre-main sequence phase (Section 1). To maximize our chances of discovering habitable worlds and life elsewhere, we must also seek observations of temperate terrestrial planets orbiting "Sun-like" (i.e., F, G, and K) stars as emphasized in the recent *Exoplanet Science Strategy* report (National Academies of Sciences & Medicine 2018). New facilities beyond those current planned would be required to accomplish these observations.

As we have shown, K dwarfs, especially later stars, offer advantages over G dwarfs in the search for biosignatures because these stars' UV spectra allow for a longer photochemical lifetime of methane in oxygenated atmospheres, thus increasing the likelihood of detecting this disequilibrium biosignature gas pair. Future observatories could target a number of nearby mid-to-late K dwarfs, including the K6V star whose spectrum we used here (HD 85512, 11.6 pc), as well as: 61 Cyg A/B (K5V/K7V, 3.5 pc; note that the 61 Cyg binaries orbit each other with a period of 544 yr; Brocksopp et al. 2002), Epsilon Indi (K4.5V, 3.6 pc), Groombridge 1618 (K7.5V, 4.8 pc), HD 156026 (K5V, 6.0 pc), Gliese 673 (K7V, 7.7 pc), HD 217357 (K7V, 8.2 pc), and HD 151288 (K7.5V, 9.8 pc). K dwarf planets orbiting these stars and others might be found by the *PLAnetary Transits and Oscillations of stars* (*PLATO*) satellite, which is expected to find K dwarf HZ planets; anticipated yields for *PLATO* of "small" planets ($R < 2$ Earth radii) in the HZ of "Sun-like" stars range from less than 10 up to 280, depending on estimates of the fraction of stars with Earth-like planets.

One challenge that K dwarfs present for direct observations is that their HZ planets will be on orbits with smaller semimajor axes compared to planets orbiting G dwarfs. This means that planets orbiting K dwarfs are more vulnerable to falling inside the IWA of future observatories. The IWA denotes the smallest planet-star separation at which a planet can be resolved and will affect the ability of any direct imaging telescope, including LUVOIR and HabEx, to observe exoplanets.

HabEx is considering designs that include a starshade, which may offer a small enough IWA to observe nearby K dwarf HZ planets. For starshades, the IWA is proportional to the radius of the starshade and inversely proportional to the starshade-telescope separation distance. The HabEx 4 m telescope starshade concept is baselined to have an IWA of 60 mas (Gaudi et al. 2018) and would be able to observe 0.3–1 μm simultaneously. Longer wavelengths out to 1.8 μm could be accessed by repositioning the starshade closer to the telescope, but this will sacrifice IWA ($IWA_{NIR} = 108$ mas). With the HabEx starshade, a planet orbiting at 0.42 au from a K6V star, such as the one that we simulate here, could be observed at

0.3–1 μm out to about 7 pc (16 pc for an Earth-equivalent planet around a G2V star) and could be observed to 1.8 μm out to about 4 pc (10 pc for a planet around a G2V star). Note, however, that the conservative HZ for a K6V star extends to 0.65 au (Kopparapu et al. 2013), so planets at the outer edge of the HZ could be observed for 0.3–1 μm out to 10 pc and for 1.8 μm out to 6 pc (26 and 15 pc, respectively, for planets at 1.6 au around a G2V star).

Both LUVOIR and HabEx are considering designs that include coronagraphs. For a coronagraph, the IWA is dependent on wavelength and inversely related to telescope diameter: IWA $= c\lambda/D$, where c is a small-valued constant of order unity, λ is wavelength, and D is telescope diameter. LUVOIR is exploring 15 m (on-axis) and 8 m (off-axis) observatory designs (LUVOIR-A and -B, respectively).

Different types of coronagraphs offer different IWAs: for instance, the apodized pupil Lyot coronagraph (APLC; Zimmerman et al. 2016) is tolerant to resolved stellar diameters but has a relatively large IWA of $\sim 3.5\lambda/D$ and takes a throughput hit from the apodizer mask. The vector vortex coronagraph (VVC; N'Diaye et al. 2015; Ruane et al. 2016) is more sensitive to resolved stars for a centrally obscured telescope aperture but offers a smaller IWA of $\sim 2\lambda/D$. The phase-induced apodization (PIAA; Guyon et al. 2010) is a third type of coronagraph that performs better for segmented apertures and offers an IWA of $\sim 3\lambda/D$. LUVOIR is exploring carrying the APLC, VVC, and/or PIAA coronagraphs on board (LUVOIR Team 2018). HabEx is baselined to carry a VVC coronagraph.

There is a moderately strong CH_4 band near 1 μm for methane-rich atmospheres such as our Case 3 planets, which might be observable for nearby K dwarfs. For our standard planet at 0.42 au from a K6V star, a coronagraph with IWA $= 3.5\lambda/D$ (APLC, only being explored by LUVOIR) could observe to 1 μm for planets at distances up to 9.5 and 5 pc for LUVOIR-A and -B, respectively (20 and 11 pc for planets around a G2V star). For a planet at the outer edge of the K6V HZ, these distance change to 13 and 7 pc for LUVOIR-A and -B (33 and 18 pc around a G2V star). Using a coronagraph with IWA $= 2\lambda/D$ (VVC, being explored by LUVOIR and HabEx), one can observe our standard K6V planet at 1 μm for distances up to 15, 8, and 4 pc for LUVOIR-A, -B, and HabEx (35, 19, and 10 pc around a G2V star). These distances change to 23, 12, and 6 pc for planets at the outer edge of the K6V HZ (55, 30, and 15 pc for planets around a G2V star, although these distances may be too far to obtain good signal).

Despite the potential challenges of observing K dwarf planets outside the IWA of possible future observatories, these stars offer the major advantage of higher planet-star contrast compared to planets orbiting G dwarf stars. Thus, their spectra can be obtained in shorter integration times. A K6V star, for instance, is only about one-tenth as bright as a G2V star (Table 1). As a comparison, a LUVOIR-A telescope observing for 50 hr can obtain a signal-to-noise ratio (S/N) of 9.2 near 1 μm for a planet orbiting a solar analog at 7 pc. This increases by more than a factor of 2 to S/N = 20 for a planet orbiting a K6V star at 7 pc. At the LUVOIR-A visible resolution, $R = 140$, Feng et al. (2018) showed that S/N = 10 at V band can provide detection (i.e., a peaked posterior distribution) of O_2, O_3, H_2O, surface pressure, and planetary radius for modern Earth, while S/N = 15 does this and provides constraints (i.e., a peaked posterior distribution with 1σ width $<$ an order of magnitude) on O_3, surface pressure, and radius (note that Feng et al. do not discuss CH_4).

Figure 4 shows simulated 50 hr (per coronagraph bandpass) LUVOIR-A observations for Case 3 planets orbiting a variety of stars in the nearby stellar neighborhood that may be targeted by future habitable planet and biosignature searches. Two nearby G dwarfs, Tau Ceti and 82 Eridani, are included for comparison. The G dwarfs use the Case 3 atmosphere generated for the Sun, and the K dwarfs use the same for the K6V star presented in Section 3. The planets orbiting the K dwarfs offer better S/N than the equivalent planets orbiting G dwarfs at similar distances due to improved planet-star contrast, and they may show stronger methane features in an O_2-rich atmosphere as highlighted here. An IWA of $2\lambda/D$ (dark gray vertical line) is sufficient to allow access to strong O_2, H_2O, CH_4, and CO_2 features for all K dwarfs shown. For the farthest stars shown, an IWA of $3.5\lambda/D$ (blue vertical line) will not allow access to CO_2 features, and CH_4 could only be detected via weaker visible wavelength bands for planets with sufficiently high CH_4 enrichment such as these Case 3 worlds.

These simulations suggest that nearby mid-to-late K dwarfs such as 61 Cyg A, and 61 Cyg B, Epsilon Indi, Groombridge 1618, and HD 156026 may be particularly excellent targets for biosignature searches on exoplanets. In addition to the "K dwarf advantage" for biosignatures, these stars can offer access to a wide range of wavelengths for HZ planets even with IWA constraints. 61 Cyg A, 61 Cyg B, Epsilon Indi, and Groombridge 1618 provide higher or comparable S/N to Tau Ceti, the closest G dwarf other than the Sun and Proxima Centauri A. In particular, 61 Cyg A and 61 Cyg B, which are at a similar distance as Tau Ceti (3.6 pc), offer S/N that is 1.6–1.7 times better in the same integration time. HD 156026 is at a similar distance as 82 Eridani (6 pc), and it offers 1.4 times better S/N compared to this G6V star.

We have shown that a sufficiently small IWA enables excellent characterization of nearby K dwarf HZ planets, so one of the most important technological innovations that could improve observations of nearby habitable K dwarf planets are observatories with small IWAs. This would provide access to redder wavelengths and/or planets orbiting more distant stars. An observatory like HabEx or LUVOIR would not launch until the 2030s or 2040s, so there is considerable time for the maturation of promising coronagraph and starshade technologies. For instance, the visible nulling coronagraph (VNC) under development offers an excellent IWA ($2\lambda/D$) with relatively high throughput due to its lack of apodizer mask, but its optical complexity is high. Technical development of the VNC is ongoing (Hicks et al. 2016).

5. Conclusions

The discovery of life on another planet would be a watershed moment in the history of science, with implications that would ripple throughout all of society. However, capturing and correctly interpreting the sparse stream of photons from distant inhabited exoplanets will be a formidable, awe-inspiring task even with powerful future telescopes.

Oxygen and methane are important gases to seek in future biosignature searches because together they indicate an atmosphere in chemical disequilibrium and are a powerful indicator of life. Previous studies have shown that the photochemical lifetime of methane in an oxygenated

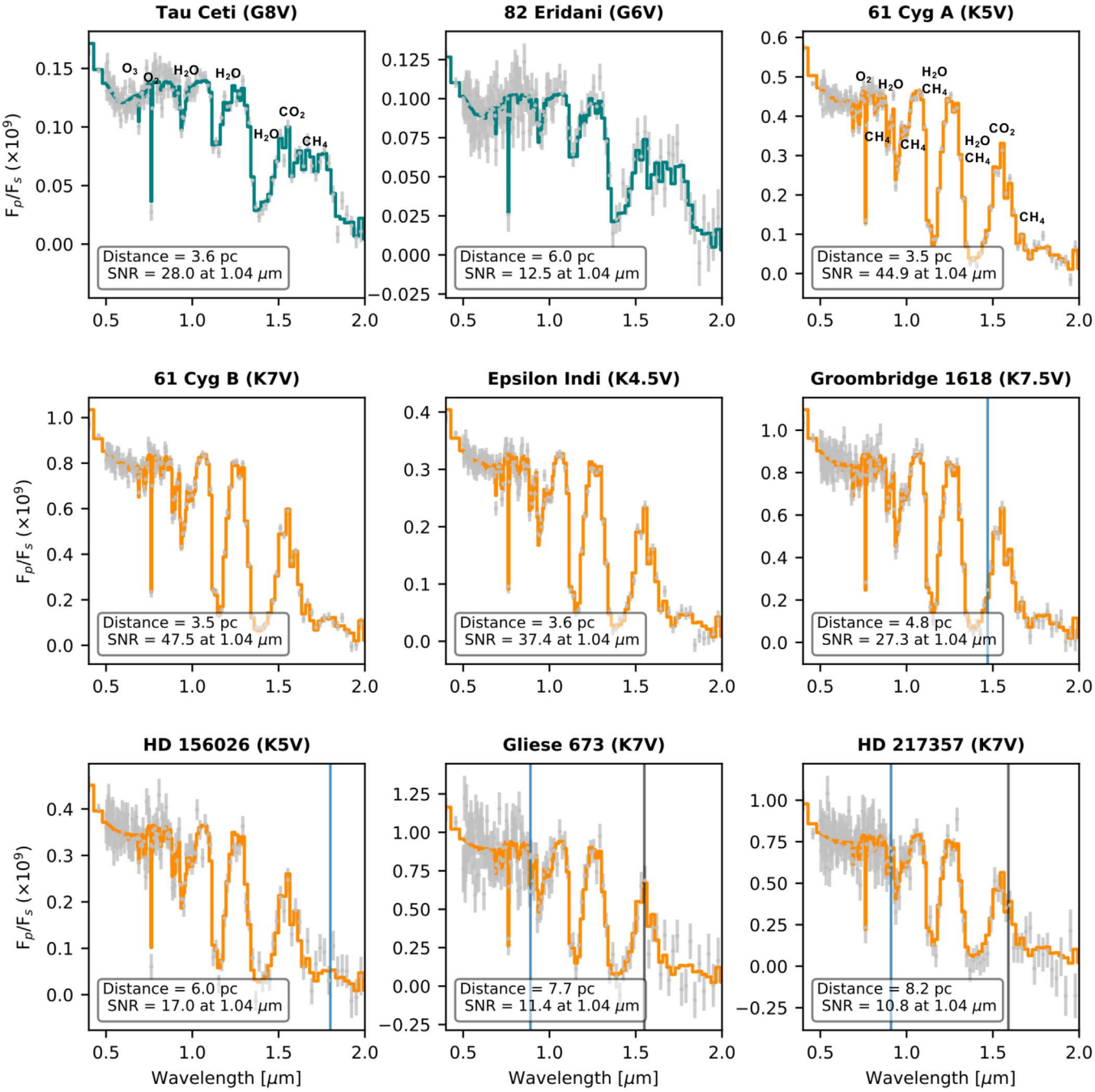

Figure 4. Simulated observations of a Case 3 planet orbiting several nearby K dwarf stars (orange spectra) that might be targeted with future exoplanet direct imaging facilities. Two nearby G dwarfs are shown for comparison (teal spectra). Important spectral features are labeled. Spectra are the same as those shown in Figure 3 for the Sun and the K6V star. Planets around all stars are placed at orbital distances where they receive 0.7× Earth's isolation. Points with error bars (gray) simulate observations with a LUVOIR-A (15 m) telescope for 50 hr of integration time per coronagraph bandpass. Vertical blue and dark gray lines show the longest wavelength that can be observed for IWA $= 3.5\lambda/D$, and IWA $= 2\lambda/D$, respectively.

atmosphere is longer around M dwarfs compared to G dwarfs. However, the habitability of M dwarf planets may be endangered by high levels of stellar activity and a prolonged superluminous pre-main sequence phase. Here, we have explored how K dwarf photochemistry can produce simultaneously observable O_2 and CH_4 spectral features, finding that later K dwarfs may generate an order of magnitude more CH_4 compared to equivalent planets around Solar-type stars. Because K dwarfs offer a better planet-star contrast ratio compared to G dwarfs, shorter observing times are needed achieve a given S/N. Particularly nearby mid-to-late K dwarfs such as 61 Cyg A/B, Epsilon Indi, Groombridge 1618, and HD 156026 may be especially good targets for future biosignature searches on exoplanets. The practical requirements for observing exoplanets in the HZs of K dwarfs should therefore be carefully considered when planning for possible future exoplanet observatories.

This work was performed as part of the NASA Astrobiology Institute's Virtual Planetary Laboratory, supported by the National Aeronautics and Space Administration through the NASA Astrobiology Institute under solicitation NNH12ZDA002C and

Cooperative Agreement Number NNA13AA93A, and by the NASA Nexus for Exoplanet System Science (NExSS) research coordination network Grant 80NSSC18K0829. We thank the Goddard Space Flight Center Sellers Exoplanet Environments Collaboration (SEEC) for support, which is funded by the NASA Planetary Science Division's Internal Scientist Funding Model (ISFM). Any opinions, findings, and conclusions or recommendations expressed in this material are those of the author(s) and do not necessarily reflect the views of NASA. The author thanks the reviewer for helpful comments that improved the quality of this manuscript.

Software: Atmos (Arney et al. 2016), SMART (Meadows & Crisp 1996), Coronagraph Noise Model (Robinson et al. 2016).

ORCID iDs

Giada N. Arney https://orcid.org/0000-0001-6285-267X

References

Airapetian, V. S., Glocer, A., Khazanov, G. V., et al. 2017, ApJL, 836, L3
Arney, G. N., Domagal-Goldman, S. D., Meadows, V. S., et al. 2016, AsBio, 16, 873
Battistuzzi, F. U., Feijao, A., & Hedges, S. B. 2004, BMC Evolutionary Biology, 4, 44
Brocksopp, C., Bode, M., Eyres, S., et al. 2002, ApJ, 571, 947
Chance, K., & Kurucz, R. 2010, JQSRT, 111, 1289
Cuntz, M., & Guinan, E. 2016, ApJ, 827, 79
Etiope, G., & Sherwood Lollar, B. 2013, RvGeo, 51, 276
Feng, Y. K., Robinson, T. D., Fortney, J. J., et al. 2018, AJ, 155, 200
France, K., Loyd, R. P., Youngblood, A., et al. 2016, ApJ, 820, 89
Garcia-Sage, K., Glocer, A., Drake, J., Gronoff, G., & Cohen, O. 2017, ApJL, 844, L13
Gaudi, B. S., Seager, S., Mennesson, B., et al. 2018, arXiv:1809.09674
Gillon, M., Triaud, A. H., Demory, B. O., et al. 2017, Natur, 542, 456
Guyon, O., Martinache, F., Belikov, R., & Soummer, R. 2010, ApJS, 190, 220
Hicks, B. A., Lyon, R. G., Bolcar, M. R., et al. 2016, Proc. SPIE, 9907, 99072O
Hitchcock, D. R., & Lovelock, J. E. 1967, Icar, 7, 149
Kaltenegger, L., Traub, W. A., & Jucks, K. W. 2007, ApJ, 658, 598
Kasting, J., & Ackerman, T. 1986, Sci, 234, 1383
Kasting, J. F., Liu, S. C., & Donahue, T. M. 1979, JGR, 84, 3097
Kharecha, P., Kasting, J., & Siefert, J. 2005, Geobiology, 3, 53
Kopparapu, R. K., Ramirez, R., Kasting, J. F., et al. 2013, ApJ, 765, 131
Krissansen-Totton, J., Bergsman, D. S., & Catling, D. C. 2016, AsBio, 16, 39
Krissansen-Totton, J., Olson, S., & Catling, D. C. 2018, SciA, 4, eaao5747
Lincowski, A. P., Meadows, V. S., Crisp, D., et al. 2018, ApJ, 867, 76
Lovelock, J. E. 1965, Natur, 207, 568
Loyd, R. P., France, K., Youngblood, A., et al. 2016, ApJ, 824, 102
Luger, R., & Barnes, R. 2015, AsBio, 15, 119
LUVOIR Team 2018, The LUVOIR Mission Concept Study Interim Report (arXiv:1809.09668)
Meadows, V., & Crisp, D. 1996, JGR, 101, 4595
Meadows, V. S., Arney, G. N., Schwieterman, E. W., et al. 2018, AsBio, 18, 133
National Academies of Sciences, E. & Medicine 2018, Exoplanet Science Strategy (Washington, DC: The National Academies Press)
N'Diaye, M., Pueyo, L., & Soummer, R. 2015, ApJ, 799, 225
Olson, S. L., Reinhard, C. T., & Lyons, T. W. 2016, PNAS, 113, 11447
Owen, J. E., & Mohanty, S. 2016, MNRAS, 459, 4088
Planavsky, N. J., Asael, D., Hofmann, A., et al. 2014a, NatGe, 7, 283
Planavsky, N. J., Reinhard, C. T., Wang, X., et al. 2014b, Sci, 346, 635
Reinhard, C. T., Olson, S. L., Schwieterman, E. W., & Lyons, T. W. 2017, AsBio, 17, 287
Richey-Yowell, T., Shkolnik, E. L., Schneider, A. C., et al. 2019, ApJ, 872, 17
Robinson, T. D., Stapelfeldt, K. R., & Marley, M. S. 2016, PASP, 128, 025003
Rosing, M. T., & Frei, R. 2004, E&PSL, 217, 237
Ruane, G., Jewell, J., Mawet, D., Pueyo, L., & Shaklan, S. 2016, Proc. SPIE, 9912, 99122L
Rugheimer, S., & Kaltenegger, L. 2018, ApJ, 854, 19
Rugheimer, S., Kaltenegger, L., Zsom, A., Segura, A., & Sasselov, D. 2013, AsBio, 13, 251
Sagan, C., Thompson, W., Carlson, R., Gurnett, D., & Hord, C. 1993, Natur, 365, 715
Schwieterman, E., Reinhard, C., Olson, S., & Lyons, T. 2018a, arXiv:1801.02744
Schwieterman, E. W., Kiang, N. Y., Parenteau, M. N., et al. 2018b, AsBio, 18, 663
Schwieterman, E. W., Robinson, T. D., Meadows, V. S., Misra, A., & Domagal-Goldman, S. 2015, ApJ, 810, 57
Segura, A., Kasting, J. F., Meadows, V., et al. 2005, AsBio, 5, 706
Segura, A., Krelove, K., Kasting, J. F., et al. 2003, AsBio, 3, 689
Shkolnik, E. L., & Barman, T. S. 2014, AJ, 148, 64
Ueno, Y., Yamada, K., Yoshida, N., Maruyama, S., & Isozaki, Y. 2006, Natur, 440, 516
Woese, C. R., & Fox, G. E. 1977, PNAS, 74, 5088
Youngblood, A., France, K., Loyd, R. P., et al. 2016, ApJ, 824, 101
Zahnle, K., Claire, M., & Catling, D. 2006, Geobiology, 4, 271
Zerkle, A. L., Claire, M. W., Domagal-Goldman, S. D., Farquhar, J., & Poulton, S. W. 2012, NatGe, 5, 359
Zimmerman, N. T., N'Diaye, M., Laurent, K. E. S., et al. 2016, Proc. SPIE, 9904, 99041Y